

Weighted Nested Commutators for Scalable Counterdiabatic State Preparation

Jiali Tang^{1,2}, Xi Chen^{1,*} and Zhi-Yuan Wei (魏志远)^{3,†}

¹*Instituto de Ciencia de Materiales de Madrid ICMM-CSIC, 28049 Madrid, Spain*

²*Departamento de Física Teórica de la Materia Condensada, Universidad Autónoma de Madrid, Madrid, Spain*

³*Joint Quantum Institute and Joint Center for Quantum Information and Computer Science, NIST/University of Maryland, College Park, Maryland 20742, USA*

Counterdiabatic (CD) driving enables efficient quantum state preparation, but it requires implementing highly nonlocal adiabatic gauge potentials (AGP) that are impractical to compute and realize in large many-body systems. We introduce a *weighted nested-commutator* (WNC) ansatz to approximate AGP using local operators. The WNC ansatz generalizes the standard nested-commutator ansatz by assigning independent variational weights to commutators of local Hamiltonian terms, thereby enlarging the variational space while preserving a fixed operator range. We show that the WNC ansatz can be efficiently optimized using a local optimization scheme. Moreover, it systematically outperforms the nested-commutator ansatz in preparing one-dimensional matrix product states (MPS) and the ground state of a nonintegrable quantum Ising model. We then numerically demonstrate that CD driving based on the WNC ansatz significantly accelerates the preparation of 1D MPS for system sizes up to $N = 1000$ qubits, as well as the two-dimensional Affleck–Kennedy–Lieb–Tasaki state on a hexagonal lattice with up to $N = 3 \times 10$ sites.

Introduction.— Adiabatic state preparation is a standard route to many-body ground states with broad applications in quantum simulation [1, 2], quantum chemistry [3], and quantum optimization algorithms [4–6]. While demonstrated across diverse scenarios [4, 7–9], it typically requires long runtimes to suppress diabatic excitations, challenging near-term devices with limited coherence. To address this issue, shortcuts to adiabaticity [10–12] have been developed to prepare the target state on substantially shorter timescales.

Counterdiabatic (CD) driving [13–17] achieves this acceleration by adding an adiabatic gauge potential (AGP) [18], that cancels nonadiabatic transitions. However, ideal CD driving requires the exact AGP, which generally depends on full eigenspectrum information and becomes highly nonlocal in many-body systems. This challenge has motivated variational constructions restricted to experimentally accessible local operators [19, 20], as well as universal schemes based on Krylov space and performance guarantees [21, 22]. The nested-commutator (NC) expansion [23–25] is a widely used ansatz for the AGP, built from a hierarchy of commutators between the Hamiltonian and its parameter derivatives, and makes CD implementations feasible [26–31].

A bottleneck of the NC ansatz is that, at any fixed truncation order, it contains only a small number of variational coefficients. This limits its expressive power, making it increasingly difficult to approximate the exact AGP as the system size grows. Improving the approximation therefore requires increasing the truncation order, which rapidly enlarges the spatial support of the resulting operators and raises both the classical optimization cost and the experimental implementation overhead [32, 33]. As a result, CD benchmarks for generic non-integrable many-body systems are often limited to system sizes ac-

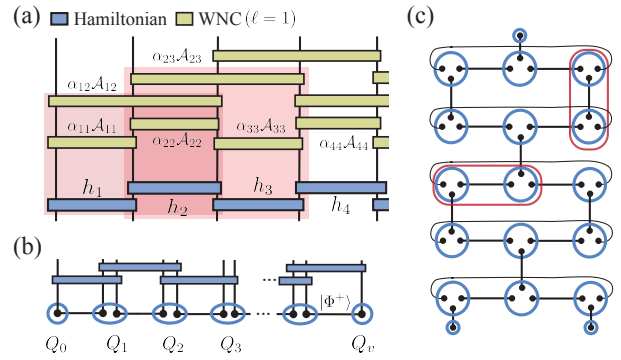


FIG. 1. (a) 1D geometrically local Hamiltonian (blue, illustrated for the nearest-neighbor case) [Eq. (1)] and the corresponding first-order ($\ell = 1$) WNC ansatz (yellow) [Eq. (5)]. In the global optimization scheme, all coefficients $\{\alpha\}$ are optimized simultaneously, whereas in the local optimization scheme the coefficients within local regions $\{\mathcal{B}_\mu\}$ (red boxes) are optimized independently. (b,c) PEPS [Eq. (10)] are constructed by contracting local tensors $\{Q_v\}$ (blue circles) with maximally entangled virtual-qudit pairs (connected dots), for both a 1D system of size $N = 2N_p$ [panel (b)] and a 2D hexagonal lattice [panel (c)], illustrated here with size $N = 3 \times 5$. The red boxes indicate the corresponding parent Hamiltonian terms [Eq. (13)].

cessible by exact diagonalization ($N \lesssim 20$ qubits).

To overcome this limitation, we introduce a weighted nested-commutator (WNC) ansatz that preserves the NC hierarchy while assigning independent variational coefficients to local commutator-string terms [Fig. 1(a)]. This yields an extensive number of variational coefficients that scale with the system size N , thereby enlarging the variational space compared to the NC ansatz at any fixed truncation order and operator range. We show that the WNC ansatz can be efficiently optimized using a local op-

timization scheme. Already at first order, WNC achieves lower infidelity than high-order NC protocols for preparing a family of matrix product states (MPS) of bond dimension $D = 2$ [Fig. 2], as well as the ground state of the nonintegrable quantum Ising model with both transverse and longitudinal field (see the *End Matter*). We further demonstrate numerically that WNC provides scalable and substantial acceleration over adiabatic state preparation for the family of 1D MPS up to system size $N = 1000$ [Fig. 3], as well as for the 2D AKLT model on a hexagonal lattice up to $N = 3 \times 10$ [Fig. 4]. These results highlight the effectiveness of WNC-based counterdiabatic driving for large many-body systems.

Model and CD driving.— We consider the quasi-adiabatic preparation of the ground state $|\psi(1)\rangle$ of a geometrically local Hamiltonian $H(1)$ on a finite-dimensional lattice of N qubits [4] with evolution time T . The system is initialized in the easy-to-prepare ground state $|\psi(0)\rangle$ of a trivial local Hamiltonian $H(0)$. With schedule function $s = s(t)$, we construct a geometrically local path $H(s)$ with $s(0) = 0$ and $s(T) = 1$. We can express the path as a sum of $N_h \sim N$ geometrically local terms $\{h_j(s)\}$, as

$$H(s) = \sum_{j=1}^{N_h \sim N} h_j(s). \quad (1)$$

The CD driving accelerates adiabatic evolution by adding the AGP $\mathcal{A}(s)$ that suppresses unwanted diabatic transitions. The resulting Hamiltonian reads [18]

$$H_{\text{CD}}(s) = H(s) + \dot{s}(t)\mathcal{A}(s), \quad (2)$$

For notational simplicity, we henceforth omit the explicit $s(t)$ dependence of H , H_{CD} , and \mathcal{A} when unambiguous. The exact AGP satisfies [18]

$$\partial_s H + \frac{i}{\hbar} [\mathcal{A}, H] = 0. \quad (3)$$

In generic interacting many-body systems, solving Eq. (3) requires full eigenspectrum information and typically yields highly nonlocal operators, making the exact AGP impractical to compute and experimentally realize.

A widely used approach is to approximate the AGP using a truncated series of nested commutators [23]. At the truncation order ℓ , we have

$$\mathcal{A}_{\text{NC}}^{(\ell)} = i \sum_{k=1}^{\ell} \alpha_k^{\text{NC}} \underbrace{[H, [H, \dots, [H, \partial_s H]]]}_{2k-1}, \quad (4)$$

where the parameters $\{\alpha_k^{\text{NC}}\}$ can be obtained variationally [19, 23] or via frequency-domain fitting [21, 22]. The NC series is systematic and recovers the exact AGP as $\ell \rightarrow \infty$ [23]. Increasing ℓ improves the accuracy but rapidly expands the operator support of each local term

in $\mathcal{A}_{\text{NC}}^{(\ell)}$, thereby increasing the associated optimization and implementation overhead of the method. Therefore, in practice, both the truncation order ℓ and the number of variational coefficients are typically small constants. This limited number of variational coefficients restricts the capability of the NC ansatz to approximate the exact AGP for large many-body systems.

WNC ansatz.— To enhance the variational power of the NC ansatz, we introduce the *weighted nested-commutator* (WNC) ansatz by assigning independent coefficients to local nested commutator terms within the NC ansatz, getting

$$\mathcal{A}_{\text{WNC}}^{(\ell)} = i \sum_{k=1}^{\ell} \sum_{j_0 \dots j_{2k-1}}^{N_h \sim N} \alpha_{j_0 \dots j_{2k-1}} \mathcal{A}_{j_0 \dots j_{2k-1}}, \quad (5)$$

with variational coefficients $\{\alpha_{j_0 \dots j_{2k-1}}\}$, and the nested commutators of local terms

$$\mathcal{A}_{j_0 \dots j_{2k-1}} = \underbrace{[h_{j_{2k-1}}, [h_{j_{2k-2}}, \dots, [h_{j_1}, \partial_s h_{j_0}]]]}_{2k-1}. \quad (6)$$

We illustrate the 1D WNC ansatz for $\ell = 1$ in Fig. 1(a).

Using the local decomposition of the Hamiltonian [Eq. (1)], it is easy to see that the NC ansatz [Eq. (4)] is a special case of the WNC ansatz by choosing $\{\alpha_{j_0 \dots j_{2k-1}}\}_{\forall j_0 \dots j_k} = \alpha_k^{\text{NC}}$ for all $k = 1, \dots, \ell$. Moreover, due to the geometric locality of the system, we expect that only $O(N)$ terms within $\{\mathcal{A}_{j_0 \dots j_{2k-1}}\}$ are non-vanishing. Nevertheless, we retain all terms formally in Eq. (5) for generality. At each fixed order ℓ , the WNC ansatz contains the same set of local nested commutator terms as the NC ansatz; therefore, the two have comparable costs for quantum implementation. However, the WNC ansatz involves significantly more variational coefficients than the NC ansatz, thereby systematically enhancing its variational expressiveness.

Variational optimization.— An established approach [19] to determine the variational coefficients (denoted as a vector $\vec{\alpha}$) within the WNC ansatz $\mathcal{A}_{\text{WNC}}^{(\ell)}(\vec{\alpha})$ is to minimize the Hilbert-Schmidt norm

$$S(\vec{\alpha}) = \left\| \partial_s H + \frac{i}{\hbar} [\mathcal{A}_{\text{WNC}}^{(\ell)}(\vec{\alpha}), H] \right\|^2, \quad (7)$$

which is equivalent in spirit to solving Eq. (3). Introducing a collective index η to label all elements within $\vec{\alpha}$, we formally rewrite $\mathcal{A}_{\text{WNC}}^{(\ell)}(\vec{\alpha}) = \sum_{\eta} \alpha_{\eta} \mathcal{A}_{\eta}$. The optimal coefficients $\vec{\alpha}_{\text{opt}}$ are obtained from the condition $\partial_{\vec{\alpha}} S(\vec{\alpha})|_{\vec{\alpha}=\vec{\alpha}_{\text{opt}}} = 0$, which yields a linear system

$$G \vec{\alpha}_{\text{opt}} = \vec{b}, \quad (8)$$

with matrix elements [34]

$$G_{\eta\eta'} = \text{Tr}(C_{\eta}^{\dagger} C_{\eta'}), \quad b_{\eta} = -\text{Tr}(C_{\eta}^{\dagger} \partial_s H), \quad (9)$$

where $C_\eta = i[\mathcal{A}_\eta, H]$. For geometrically local Hamiltonians on finite-dimensional lattices, commutators between terms that do not spatially overlap vanish, thus each matrix element in Eq. (9) can be evaluated in a time independent of the system size N . Moreover, the number of non-vanishing terms [cf. Eq. (6)] in the WNC ansatz, i.e., the dimension of the linear system Eq. (8), scales as $O(N)$. Therefore, the optimal coefficients $\vec{\alpha}_{\text{opt}}$ can be obtained with a computational cost $O(N^3)$ [34]. We refer to this procedure as the *global optimization*.

To further reduce the optimization cost, we propose a *local optimization* strategy. Specifically, we partition the system into $O(N)$ geometrically local regions $\{\mathcal{B}_\mu\}$ that cover the full lattice [cf. Fig. 1(a)]. For each region \mathcal{B}_μ , we define $H_{\mathcal{B}_\mu}$ as the sum of all Hamiltonian terms in H [Eq. (1)] that are supported within \mathcal{B}_μ . Similarly, we construct $\mathcal{A}_{\text{WNC}}^{(\ell, \mathcal{B}_\mu)}$ by summing the nested commutators of local terms supported in \mathcal{B}_μ . We then construct the action in the same manner as in Eq. (7), but with the Hamiltonian and the WNC ansatz replaced by their local counterparts, $H_{\mathcal{B}_\mu}$ and $\mathcal{A}_{\text{WNC}}^{(\ell, \mathcal{B}_\mu)}$. Applying the same procedure as in Eqs. (8) and (9), we obtain the coefficients associated with the WNC terms supported within \mathcal{B}_μ . Scanning over $\{\mathcal{B}_\mu\}$ that cover the full lattice, we determine all coefficients. Note that, certain coefficients will get different locally optimized values due to the potential overlap of the local regions $\{\mathcal{B}_\mu\}$ [e.g. the term $\alpha_{22}A_{22}$ in Fig. 1(a)], and we average these values. The local optimization approach reduces the scaling of the computational overhead from $O(N^3)$ to $O(N)$ [34].

PEPS and adiabatic path.— In the remainder of this work, we apply CD driving based on the WNC ansatz to accelerate the adiabatic preparation of projected entangled pair states (PEPS), following the same adiabatic path studied in Ref. [35]. In the following, we briefly review PEPS and the associated adiabatic path [35].

We consider a PEPS on a graph \mathcal{G} , with edges \mathcal{E} and vertices \mathcal{V} , written as

$$|\psi_{\text{PEPS}}\rangle \propto \bigotimes_{v \in \mathcal{V}} Q_v \bigotimes_{e \in \mathcal{E}} |\Phi^+\rangle_e, \quad (10)$$

where Q_v acts on the maximally entangled state $|\Phi^+\rangle_e \propto \sum_{\alpha=0}^{D-1} |\alpha\alpha\rangle$ with bond dimension D of PEPS [cf. Fig. 1(b,c)]. The MPS can be viewed as 1D PEPS with 2 virtual qudits per site, with Q_v in the bulk takes the following form:

$$Q_v^{\text{1D}} = \sum_{i_v=0}^{d-1} \sum_{\alpha_v, \beta_v=0}^{D-1} A_{[v]\alpha_v\beta_v}^{i_v} |i_v\rangle \langle \alpha_v\beta_v|, \quad (11)$$

where $A_{[v]}^{i_v}$ represents the MPS tensors. If the $\{Q_v\}$ are left-invertible, a PEPS is called *injective*.

The first example we study is the $D = 2$ MPS family [cf. Fig. 1(b)] introduced in Ref. [36], and subsequently used as a benchmark in various studies [35, 37–42]. By

grouping neighboring pairs within the bulk of $N = 2N_p$ qubits into N_p qudits of dimension $d = 4$ [cf. Fig. 1(b)], we obtain an injective MPS with physical dimension $d = D^2 = 4$. The corresponding tensor in Eq. (11) is

$$\begin{aligned} A_{[v]}^0(g) &= \begin{pmatrix} 0 & 0 \\ 1 & 1 \end{pmatrix}, & A_{[v]}^1(g) &= \begin{pmatrix} 0 & 0 \\ 1 & g \end{pmatrix}, & (12) \\ A_{[v]}^2(g) &= \begin{pmatrix} g & g \\ 0 & 0 \end{pmatrix}, & A_{[v]}^3(g) &= \begin{pmatrix} 1 & g \\ 0 & 0 \end{pmatrix}. \end{aligned}$$

We focus on $g < 0$, where this MPS family exhibit symmetry-protected topological (SPT) order, interpolating between the cluster state at $g = -1$ and the GHZ state at $g = 0$ [36, 37]. By tuning g , one can control the

correlation length of the state as $\xi = \left| \ln \left(\frac{1-g}{1+g} \right) \right|^{-1}$.

Another example we consider is the 2D AKLT state on a hexagonal lattice with cylinder boundary condition [cf. Fig. 1(c)], which exhibits weak SPT order [43] and serves as a universal resource for measurement-based quantum computation [44]. The AKLT state can be expressed as an injective PEPS with bond dimension $D = 2$ [34]. It can be prepared deterministically using adiabatic algorithms [35, 45, 46], or probabilistically via measurement-based protocols [47, 48].

To get an adiabatic path, we construct a PEPS interpolation $|\psi(s)\rangle$ [cf. Eq. 10] with tensors $Q_v(s) = sQ_v + (1-s)\mathbb{1}$ with $s \in [0, 1]$, which connects the product state of maximally entangled pairs $|\psi(0)\rangle = \bigotimes_{e \in \mathcal{E}} |\Phi^+\rangle_e$ to the target state $|\psi(1)\rangle \equiv |\psi_{\text{PEPS}}\rangle$. The parent Hamiltonian of $|\psi(s)\rangle$ is [35, 36, 49] [cf. Fig. 1(b)]

$$H(s) = \sum_e \Pi_{\text{ker}}[\rho_e(s)], \quad (13)$$

where each term $\Pi_{\text{ker}}[\rho_e(s)]$ denotes the projector onto the kernel of the reduced density matrix $\rho_e(s)$ on edge e , and will be identified as a local term in Eq. (1).

For all examples, the time-dependent variational principle (TDVP) is used for numerical simulation [34]. We compute the fidelity $\mathcal{F} = |\langle \psi(1) | \phi(T) \rangle|^2$ between the evolved state $|\phi(T)\rangle$ for time T and the target ground state $|\psi(1)\rangle$. We adopt the schedule function $s_{\text{1D}}(t) = \sin^2 \left[\frac{\pi}{2} \sin^2 \left(\frac{\pi t}{2T} \right) \right]$ for the 1D MPS family, and $s_{\text{2D}}(t) = \sin^2(\pi t / 2T)$ for the 2D AKLT state [35].

Benchmarking WNC.— To benchmark the WNC ansatz, we study the preparation of the 1D MPS family with system size $N = 30$ using the adiabatic evolution [cf. Eq. (1)] and the CD-assisted evolution [cf. (2)] using either the high-order NC or first-order WNC ansatz.

For a fixed correlation length $\xi \approx 3.8$ of the target state, Fig. 2(a) shows that, compared to adiabatic evolution, CD driving based on the NC ansatz systematically reduces the infidelity as the truncation order ℓ increases. Moreover, the WNC ansatz, based on either global or local optimization, yields a significantly lower infidelity

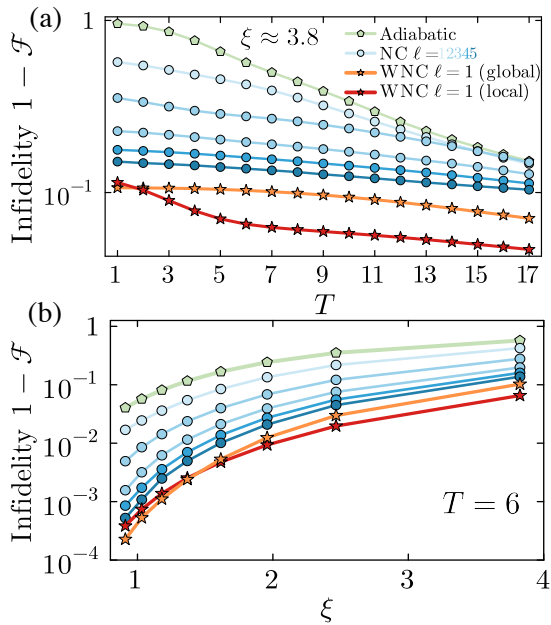


FIG. 2. Preparation of the MPS family [Eq. (12)] of $N = 30$ using adiabatic evolution and CD driving based on the NC and WNC ansatz. (a) Infidelity as a function of the total evolution time T for a fixed target-state correlation length $\xi \approx 3.8$. (b) Infidelity as a function of ξ for a fixed $T = 6$.

than the NC ansatz: the first-order WNC ansatz already outperforms the fifth-order NC ansatz across the entire range of T .

Fixing time $T = 6$, Fig. 2(b) further demonstrates that the advantage of the first-order WNC ansatz over up to fifth-order NC ansatz persists across target states with different correlation lengths. In particular, within the same evolution time, the first-order WNC ansatz achieves nearly a three-order-of-magnitude reduction in infidelity compared to adiabatic evolution. The speedup is more pronounced for states with shorter correlation lengths, as the finite speed of information propagation limits how much states with longer correlations can be accelerated within a fixed evolution time. Finally, in the *End Matter*, we show that the first-order WNC ansatz likewise outperforms the high-order NC ansatz in preparing the ground state of a 1D non-integrable quantum Ising model.

These results demonstrate that the additional variational degrees of freedom in the WNC ansatz significantly enhance the state-preparation performance compared to the NC ansatz. We further show in the SM that, for digital Hamiltonian simulation using first-order Trotterization, CD driving based on the first-order WNC ansatz achieves high-fidelity state preparation with far fewer gates than either adiabatic evolution or CD driving based on the high-order NC ansatz [34]. Moreover, the local optimization scheme is found to be both computationally more efficient and capable of achieving lower infidelity overall. In the following, we therefore adopt the WNC

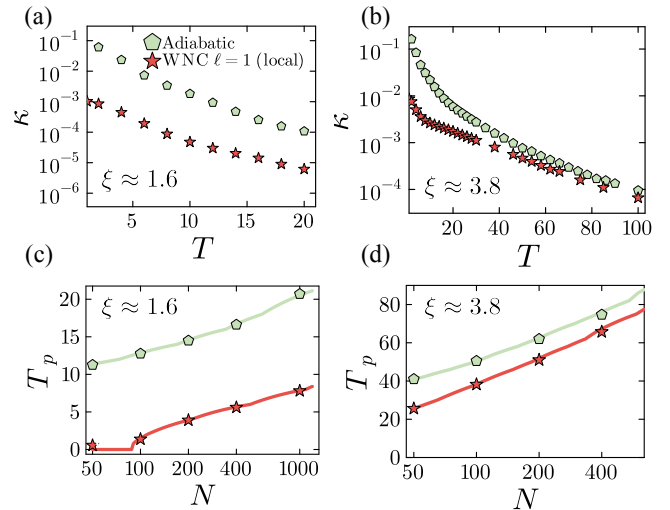


FIG. 3. (a),(b) Extracted error density $\kappa(T)$ [cf. Eq. (14)] versus the evolution time T for the preparation of the MPS family with correlation lengths $\xi \approx 1.6, 3.8$. (c),(d) Runtime T_p required to reach the target fidelity $\mathcal{F} = 0.95$ for the 1D MPS family preparation as a function of system size N . Solid green (adiabatic) and red (WNC) lines show the prediction from Eq. (14), and symbols denote TDVP simulation results.

ansatz with local optimization to study the CD-assisted preparation of large-scale many-body ground states.

Large-scale preparation of 1D MPS.— For large-scale quasi-adiabatic state preparation, it has been shown that the fidelity $\mathcal{F}(N, T)$ exhibit an exponential decay with the system size N [35]

$$\mathcal{F}(N, T) = \exp[-\kappa(T) \cdot N - c(T)], \quad (14)$$

with error density $\kappa(T)$ reduces when increasing the evolution time T , together with a system-size independent term $c(T)$ induced by the boundary effects.

Under CD driving based on the WNC ansatz ($\ell = 1$), the fidelity exhibits the same scaling behavior as in Eq. (14), but with a reduced error density $\kappa(T)$ [34]. The extracted $\kappa(T)$ for the preparation of the MPS family is presented in Fig. 3(a,b). For a short correlation length $\xi \approx 1.6$, CD driving based on the WNC ansatz reduces $\kappa(T)$ by nearly two orders of magnitude. For a longer correlation length $\xi \approx 3.8$, the reduction is more pronounced at short evolution times and gradually vanishes at large T , where the system approaches the adiabatic limit. This behavior is expected, as the derivative $\dot{s}(t)$ in Eq. (2) becomes negligible in the large- T limit.

Using Eq. (14), one can predict the required evolution time T_p to prepare an N -particle state with a desired target fidelity. In Fig. 3(c,d), we present the predicted T_p for preparing the MPS family with $\mathcal{F} = 0.95$, and compare it with TDVP simulations of the evolution for system sizes up to $N = 1000$, finding excellent agreement. For example, for $\xi \approx 1.6$ and a fixed evolution-time budget of $T_p \approx 10$, CD driving based on the WNC ansatz

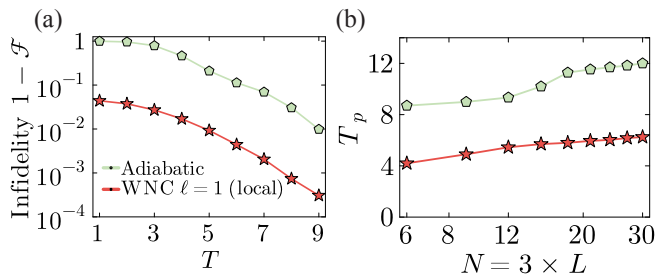


FIG. 4. (a) In-fidelity of preparing the 2D AKLT state on the hexagonal lattice ($N = 3 \times 3$) as a function of the total evolution time T . (b) The evolution time T_p required to prepare the 2D AKLT state on a hexagonal lattice with fidelity $\mathcal{F} = 0.99$ for system sizes $N = 3 \times L$ ($L = 3 - 10$) for adiabatic evolution and the CD driving based on the WNC ansatz ($\ell = 1$).

($\ell = 1$) can prepare states of a size nearly two orders of magnitude larger than those achievable via adiabatic evolution. Additional results for $\xi \approx 0.9, 2.5$, together with the extracted $c(T)$, are provided in the SM [34].

2D AKLT states.— Going beyond 1D systems, we present numerical results for preparing the 2D AKLT state on a hexagonal lattice [cf. Fig. 1(c)] with system size $N = 3 \times L$ in Fig. 4. For a fixed size $N = 3 \times 3$ [panel (a)], the CD driving based on the WNC ansatz ($\ell = 1$) reduces the state-preparation infidelity by more than an order of magnitude compared to adiabatic evolution across the entire range of evolution times T . For a target fidelity $\mathcal{F} = 0.99$ [panel (b)], the CD driving based on the WNC ansatz approximately halves the required evolution time T_p for lattices up to $N = 3 \times 10$ sites (each bulk site contains three qubits), which is well beyond the reach of exact diagonalization.

Discussions.— We introduced the WNC ansatz together with a local optimization scheme for tuning its parameters, and showed that it systematically outperforms the standard NC ansatz. Our numerical results demonstrate that CD driving based on the WNC ansatz can significantly accelerate the adiabatic preparation of large interacting many-body ground states in both 1D systems (up to $N = 1000$) and 2D lattices (up to $N = 3 \times 10$, with three qubits per site).

Promising future directions include numerically exploring higher-order WNC ansatz to further enhance performance and clarify their scaling properties; designing experimental implementations of WNC on near-term quantum platforms [17, 23, 50]; developing analytical or semi-analytical methods for determining the WNC coefficients, potentially with provable performance guarantees [21, 22]; extending the WNC ansatz to the preparation of gapless ground states [51, 52] and long-range entangled phases [53]; and devising hybrid acceleration strategies that combine WNC ansatz with complementary approaches such as optimal control, measurement-

induced cooling [54] and machine-learning-based techniques [12].

ACKNOWLEDGMENTS

We thank Andrew Childs and Daniel Malz for insightful discussions. XC is supported by project Grant No. PID2021-125823NA-I00 funded by MCIN/AEI/10.13039/501100011033 and by “ERDF A way of making Europe” and “ERDF Invest in your Future”, Basque Government through Grant No. IT1470-22, and the Severo Ochoa Centres of Excellence program through Grant CEX2024-001445-S. ZYW is supported in part by the NSF STAQ program.

* xi.chen@csic.es

† zywei@umd.edu

- [1] I. M. Georgescu, S. Ashhab, and F. Nori, Quantum simulation, *Rev. Mod. Phys.* **86**, 153 (2014).
- [2] A. J. Daley, I. Bloch, C. Kokail, S. Flannigan, N. Pearson, M. Troyer, and P. Zoller, Practical quantum advantage in quantum simulation, *Nature* **607**, 667 (2022).
- [3] S. McArdle, S. Endo, A. Aspuru-Guzik, S. C. Benjamin, and X. Yuan, Quantum computational chemistry, *Rev. Mod. Phys.* **92**, 015003 (2020).
- [4] T. Albash and D. A. Lidar, Adiabatic quantum computation, *Rev. Mod. Phys.* **90**, 015002 (2018).
- [5] B. F. Schiffer, J. Tura, and J. I. Cirac, Adiabatic spectroscopy and a variational quantum adiabatic algorithm, *PRX Quantum* **3**, 020347 (2022).
- [6] A. Abbas, A. Ambainis, B. Augustino, A. Bäertschi, H. Buhrman, C. Coffrin, G. Cortiana, V. Dunjko, D. J. Egger, B. G. Elmegreen, N. Franco, F. Fratini, B. Fuller, J. Gacon, C. Gonciulea, S. Gribling, S. Gupta, S. Hadfield, R. Heese, G. Kircher, T. Kleinert, T. Koch, G. Korpas, S. Lenk, J. Marecek, V. Markov, G. Mazzola, S. Mensa, N. Mohseni, G. Nannicini, C. O’Meara, E. P. Tapia, S. Pokutta, M. Proissl, P. Rebentrost, E. Sahin, B. C. B. Symons, S. Tornow, V. Valls, S. Woerner, M. L. Wolf-Bauwens, J. Yard, S. Yarkoni, D. Zechiel, S. Zhuk, and C. Zoufal, Challenges and opportunities in quantum optimization, *Nat. Rev. Phys.* **6**, 718–735 (2024).
- [7] R. Menchon-Enrich, A. Benseny, V. Ahufinger, A. D. Greentree, T. Busch, and J. Mompart, Spatial adiabatic passage: a review of recent progress, *Reports on Progress in Physics* **79**, 074401 (2016).
- [8] N. V. Vitanov, A. A. Rangelov, B. W. Shore, and K. Bergmann, Stimulated raman adiabatic passage in physics, chemistry, and beyond, *Rev. Mod. Phys.* **89**, 015006 (2017).
- [9] C. P. Koch, U. Boscain, T. Calarco, G. Dirr, S. Filipp, S. J. Glaser, R. Kosloff, S. Montangero, T. Schulte-Herbrüggen, D. Sugny, *et al.*, Quantum optimal control in quantum technologies. strategic report on current status, visions and goals for research in europe, *EPJ Quantum Technology* **9**, 19 (2022).

- [10] X. Chen, A. Ruschhaupt, S. Schmidt, A. del Campo, D. Guéry-Odelin, and J. G. Muga, Fast optimal frictionless atom cooling in harmonic traps: Shortcut to adiabaticity, *Phys. Rev. Lett.* **104**, 063002 (2010).
- [11] D. Guéry-Odelin, A. Ruschhaupt, A. Kiely, E. Torrontegui, S. Martínez-Garaot, and J. G. Muga, Shortcuts to adiabaticity: Concepts, methods, and applications, *Rev. Mod. Phys.* **91**, 045001 (2019).
- [12] C. W. Duncan, P. M. Poggi, M. Bukov, N. T. Zinner, and S. Campbell, Taming quantum systems: A tutorial for using shortcuts-to-adiabaticity, quantum optimal control, and reinforcement learning, *PRX Quantum* **6**, 040201 (2025).
- [13] M. V. Berry, Transitionless quantum driving, *J. Phys. A Math. Theor.* **42**, 365303 (2009).
- [14] X. Chen, I. Lizuain, A. Ruschhaupt, D. Guéry-Odelin, and J. G. Muga, Shortcut to adiabatic passage in two- and three-level atoms, *Phys. Rev. Lett.* **105**, 123003 (2010).
- [15] A. del Campo, Shortcuts to adiabaticity by counterdiabatic driving, *Phys. Rev. Lett.* **111**, 100502 (2013).
- [16] N. N. Hegade, K. Paul, Y. Ding, M. Sanz, F. Albarrán-Arriagada, E. Solano, and X. Chen, Shortcuts to adiabaticity in digitized adiabatic quantum computing, *Phys. Rev. Appl.* **15**, 024038 (2021).
- [17] P. M. Schindler and M. Bukov, Counterdiabatic driving for periodically driven systems, *Phys. Rev. Lett.* **133**, 123402 (2024).
- [18] M. Kolodrubetz, D. Sels, P. Mehta, and A. Polkovnikov, Geometry and non-adiabatic response in quantum and classical systems, *Phys. Rep.* **697**, 1 (2017).
- [19] D. Sels and A. Polkovnikov, Minimizing irreversible losses in quantum systems by local counterdiabatic driving, *Proceedings of the National Academy of Sciences* **114**, E3909 (2017).
- [20] I. Čepaitė, A. Polkovnikov, A. J. Daley, and C. W. Duncan, Counterdiabatic optimized local driving, *PRX Quantum* **4**, 010312 (2023).
- [21] J. R. Finžgar, S. Notarnicola, M. Cain, M. D. Lukin, and D. Sels, Counterdiabatic driving with performance guarantees, *Phys. Rev. Lett.* **135**, 180602 (2025).
- [22] S. Morawetz and A. Polkovnikov, Universal counterdiabatic driving in krylov space, *PRX Quantum* **6**, 040320 (2025).
- [23] P. W. Claeys, M. Pandey, D. Sels, and A. Polkovnikov, Floquet-engineering counterdiabatic protocols in quantum many-body systems, *Phys. Rev. Lett.* **123**, 090602 (2019).
- [24] B. Bhattacharjee, A lanczos approach to the adiabatic gauge potential (2023), [arXiv:2302.07228 \[quant-ph\]](https://arxiv.org/abs/2302.07228).
- [25] K. Takahashi and A. del Campo, Shortcuts to adiabaticity in krylov space, *Phys. Rev. X* **14**, 011032 (2024).
- [26] Y.-X. Du, Z.-T. Liang, Y.-C. Li, X.-X. Yue, H. Yan, and S.-L. Zhu, Experimental realization of stimulated raman shortcut-to-adiabatic passage with cold atoms, *Nature Communications* **7**, 12479 (2016).
- [27] S. An, D. Lv, A. Del Campo, and K. Kim, Shortcuts to adiabaticity by counterdiabatic driving for trapped-ion displacement in phase space, *Nature communications* **7**, 12999 (2016).
- [28] Z. Zhan, C. Run, Z. Zong, L. Xiang, Y. Fei, Z. Sun, Y. Wu, Z. Jia, P. Duan, J. Wu, Y. Yin, and G. Guo, Experimental determination of electronic states via digitized shortcut to adiabaticity and sequential digitized adiabaticity, *Phys. Rev. Appl.* **16**, 034050 (2021).
- [29] H. Zhou, Y. Ji, X. Nie, X. Yang, X. Chen, J. Bian, and X. Peng, Experimental realization of shortcuts to adiabaticity in a nonintegrable spin chain by local counterdiabatic driving, *Phys. Rev. Appl.* **13**, 044059 (2020).
- [30] H. Zhou, X. Dai, J. Geng, Y. Ji, and X. Peng, Approximate constructions of counterdiabatic driving with nm quantum systems, *Chinese Physics B* **33**, 090301 (2024).
- [31] H. Guan, F. Zhou, F. Albarrán-Arriagada, X. Chen, E. Solano, N. N. Hegade, and H.-L. Huang, Single-layer digitized-counterdiabatic quantum optimization for p-spin models, *Quantum Science and Technology* **10**, 015006 (2024).
- [32] G. Passarelli and P. Lucignano, Counterdiabatic reverse annealing, *Phys. Rev. A* **107**, 022607 (2023).
- [33] S. Morawetz and A. Polkovnikov, Efficient paths for local counterdiabatic driving, *Phys. Rev. B* **110**, 024304 (2024).
- [34] See Supplemental Material at [URL will be inserted by publisher] for more details.
- [35] Z.-Y. Wei, D. Malz, and J. I. Cirac, Efficient adiabatic preparation of tensor network states, *Phys. Rev. Res.* **5**, L022037 (2023).
- [36] M. M. Wolf, G. Ortiz, F. Verstraete, and J. I. Cirac, Quantum phase transitions in matrix product systems, *Phys. Rev. Lett.* **97**, 110403 (2006).
- [37] A. Smith, B. Jobst, A. G. Green, and F. Pollmann, Crossing a topological phase transition with a quantum computer, *Phys. Rev. Res.* **4**, L022020 (2022).
- [38] K. C. Smith, A. Khan, B. K. Clark, S. Girvin, and T.-C. Wei, Constant-depth preparation of matrix product states with adaptive quantum circuits, *PRX Quantum* **5**, 030344 (2024).
- [39] D. Malz, G. Styliaris, Z.-Y. Wei, and J. I. Cirac, Preparation of matrix product states with log-depth quantum circuits, *Phys. Rev. Lett.* **132**, 040404 (2024).
- [40] Z.-Y. Wei and D. Malz, State preparation with parallel-sequential circuits (2025), [arXiv:2503.14645 \[quant-ph\]](https://arxiv.org/abs/2503.14645).
- [41] M. Scheer, A. Baiardi, E. B. Marty, Z.-Y. Wei, and D. Malz, Renormalization-group-based preparation of matrix product states on up to 80 qubits (2025), [arXiv:2510.24681 \[quant-ph\]](https://arxiv.org/abs/2510.24681).
- [42] L. E. Fischer, D. Bultrini, I. Tavernelli, and F. Tacchino, Large-scale implementation of quantum subspace expansion with classical shadows (2025), [arXiv:2510.25640 \[quant-ph\]](https://arxiv.org/abs/2510.25640).
- [43] Y.-Z. You, Z. Bi, A. Rasmussen, K. Slagle, and C. Xu, Wave function and strange correlator of short-range entangled states, *Phys. Rev. Lett.* **112**, 247202 (2014).
- [44] T. C. Wei, I. Affleck, and R. Raussendorf, Affleck-Kennedy-Lieb-Tasaki State on a honeycomb lattice is a universal quantum computational resource, *Physical Review Letters* **106**, 1 (2011).
- [45] M. Schwarz, K. Temme, and F. Verstraete, Preparing projected entangled pair states on a quantum computer, *Phys. Rev. Lett.* **108**, 110502 (2012).
- [46] Y. Ge, A. Molnár, and J. I. Cirac, Rapid adiabatic preparation of injective projected entangled pair states and gibbs states, *Phys. Rev. Lett.* **116**, 080503 (2016).
- [47] B. Murta, P. M. Q. Cruz, and J. Fernández-Rossier, Preparing Valence-Bond-Solid states on noisy intermediate-scale quantum computers (2022).
- [48] W. Guo, M. Litvinov, T.-C. Wei, A. Khan, and K. C. Smith, Measurement-based preparation of higher-

dimensional aklt states and their quantum computational power (2026), arXiv:2602.07201 [quant-ph].

- [49] D. Perez-Garcia, F. Verstraete, J. I. Cirac, and M. M. Wolf, *Peps as unique ground states of local hamiltonians* (2007), arXiv:0707.2260 [quant-ph].
- [50] E. Boyers, M. Pandey, D. K. Campbell, A. Polkovnikov, D. Sels, and A. O. Sushkov, Floquet-engineered quantum state manipulation in a noisy qubit, *Phys. Rev. A* **100**, 012341 (2019).
- [51] A. Polkovnikov, Universal adiabatic dynamics in the vicinity of a quantum critical point, *Phys. Rev. B* **72**, 161201 (2005).
- [52] A. Grabarits, F. Balducci, and A. del Campo, Fighting exponentially small gaps by counterdiabatic driving, *PRX Quantum* **7**, 010322 (2026).
- [53] N. O. Gjonbalaj, R. Sahay, and S. F. Yelin, Shortcuts to analog preparation of non-equilibrium quantum lakes (2025), arXiv:2502.03518 [quant-ph].
- [54] J. Langbehn, K. Snizhko, I. Gornyi, G. Morigi, Y. Gefen, and C. P. Koch, Dilute measurement-induced cooling into many-body ground states, *PRX Quantum* **5**, 030301 (2024).

END MATTER: BENCHMARK FOR QUANTUM ISING MODEL

As an additional benchmark, we apply the CD driving based on the WNC ansatz ($\ell = 1$) to the non-integrable quantum Ising model with both transverse and longitudinal field,

$$H(1) = h_z \sum_{j=1}^N Z_j + h_x \sum_{j=1}^N X_j + J \sum_{j=1}^{N-1} Z_j Z_{j+1}, \quad (15)$$

where $\{X_j\}$ and $\{Z_j\}$ are Pauli operators.

We consider the following linear Hamiltonian interpolation that connects the trivial initial Hamiltonian $H(0) = h_z \sum_{j=1}^N Z_j$ to $H(1)$, as

$$H(s) = (1-s) h_z \sum_{j=1}^N Z_j + s \left(h_x \sum_{j=1}^N X_j + J \sum_{j=1}^{N-1} Z_j Z_{j+1} \right), \quad (16)$$

with schedule function $s(t) = \sin^2\left(\frac{\pi}{2} \sin^2\left(\frac{\pi t}{2T}\right)\right)$, and the parameters $J = 1, h_x = 2, h_z = 1$.

At first order ($\ell = 1$), the local nested commutators terms within the WNC ansatz [Eq. (5)] yield a minimal set of local operators consisting of single-site $\{Y_j\}$ and two-body operators $\{Y_j Z_{j+1}\}$ and $\{Z_j Y_{j+1}\}$. Assigning

independent coefficients to each local string, the first-order WNC ansatz is

$$\mathcal{A}_{\text{WNC, Ising}}^{(\ell=1)} = \sum_{j=1}^N \alpha_j^y Y_j + \sum_{j=1}^{N-1} \left(\alpha_j^{yz} Y_j Z_{j+1} + \alpha_j^{zy} Z_j Y_{j+1} \right), \quad (17)$$

with coefficients $\{\alpha_j^y, \alpha_j^{yz}, \alpha_j^{zy}\}$. We employ the same global and local optimization schemes described in the main text to obtain the optimal coefficients. In the local scheme, the regions consist of three neighboring sites $(j, j+1, j+2)$ for $j = 1, \dots, N-2$.

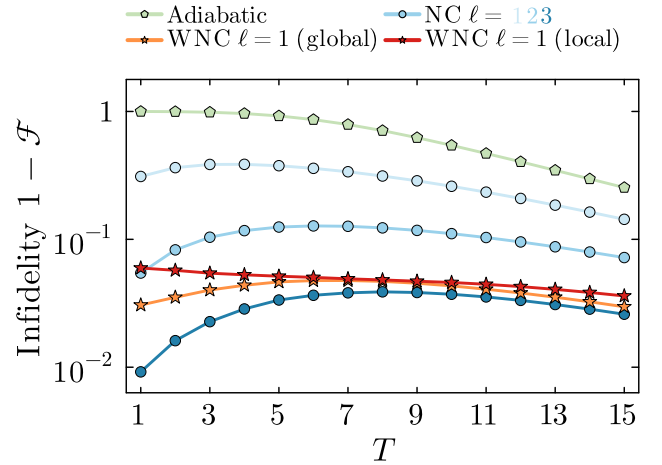


FIG. 5. Infidelity for preparing the ground state of (15) along the path (16) as a function of total time T . Parameters: $h_x = 2, h_z = J = 1, N = 15$.

We simulate the evolution along the path in Eq. (16) for $N = 15$ with $h_x = 2$ and $h_z = J = 1$, and compare (i) adiabatic evolution, (ii) CD driving based on the NC ansatz at truncation orders $\ell = 1, 2, 3$, and (iii) first-order WNC with both global and local optimization.

The results are shown in Fig. 5. Similar to the preparation of the 1D MPS family [cf. Fig. 2], the first-order WNC ansatz already achieves an infidelity comparable to that of the high-order NC ansatz ($\ell = 3$ in this case). Moreover, the performance of the local optimization closely matches that of the global optimization, indicating that the local scheme offers both improved optimization efficiency and competitive state-preparation performance.

Supplementary Materials for: Weighted Nested Commutators for Scalable Counterdiabatic State Preparation

Jialiang Tang ^{1,2} Xi Chen ^{1,*} and Zhi-Yuan Wei (魏志远) ^{3,†}

¹*Instituto de Ciencia de Materiales de Madrid ICMM-CSIC, 28049 Madrid, Spain*

²*Departamento de Física Teórica de la Materia Condensada,
Universidad Autónoma de Madrid, Madrid, Spain*

³*Joint Quantum Institute and Joint Center for Quantum Information and Computer Science,
NIST/University of Maryland, College Park, Maryland 20742, USA*

CONTENTS

S1. Optimizing the variational coefficients	1
A. The optimization scheme	1
B. Scaling of the optimization cost	2
1. Global optimization	2
2. Local optimization	2
S2. 2D AKLT state on the hexagonal lattice	3
S3. Numerical simulation details	3
S4. Additional Results on the preparation of the 1D MPS Family	4
A. Scaling of the Fidelity with system size N	4
B. More Results for different correlation lengths, and the boundary term $c(T)$	4
C. Comparing gate costs in Trotterized simulations of various state-preparation schemes	5
References	6

S1. OPTIMIZING THE VARIATIONAL COEFFICIENTS

Here we provide more details on the optimization scheme used to optimize the parameters in the weighted nested commutator (WNC) ansatz [Eq.(5) in the main text], and discuss the associated computational cost. The same optimization procedure is also applied to determine the coefficients in the standard nested commutator (NC) ansatz [Eq.(4) in the main text] studied in this paper.

A. The optimization scheme

For the WNC ansatz, each non-vanishing nested commutator of local terms [Eq.(6) in the main text] has an independent parameter, which we collectively denote as $\mathcal{A}_{\text{WNC}}^{(\ell)}(\vec{\alpha}) = \sum_{\eta} \alpha_{\eta} \mathcal{A}_{\eta}$. The optimal coefficients $\vec{\alpha}_{\text{opt}}$ can be determined by minimizing the Hilbert-Schmidt norm [S1]

$$S(\vec{\alpha}) = \left\| \partial_s H + \frac{i}{\hbar} [\mathcal{A}_{\text{WNC}}^{(\ell)}(\vec{\alpha}), H] \right\|^2, \quad (\text{S1})$$

where $\|O\|^2 := \text{Tr}(O^\dagger O)$. We set $\hbar = 1$ from now on.

Defining $C_{\eta} := i[\mathcal{A}_{\eta}, H]$, we can expand $S(\vec{\alpha})$ as

$$S(\vec{\alpha}) = \text{Tr} \left[\partial_s H^\dagger \partial_s H \right] + 2 \sum_{\eta} \alpha_{\eta} \text{Tr} \left(C_{\eta}^\dagger \partial_s H \right) + \sum_{\eta, \eta'} \alpha_{\eta} \alpha_{\eta'} \text{Tr} \left(C_{\eta}^\dagger C_{\eta'} \right). \quad (\text{S2})$$

* xi.chen@csic.es

† zywei@umd.edu

Further defining the positive semi-definite Gram matrix G and the vector \vec{b} , with elements

$$G_{\eta\eta'} = \text{Tr}(C_\eta^\dagger C_{\eta'}), \quad b_\eta = -\text{Tr}(C_\eta^\dagger \partial_s H). \quad (\text{S3})$$

With that, the stationarity condition $\partial_{\vec{\alpha}} S(\vec{\alpha})|_{\vec{\alpha}=\vec{\alpha}_{\text{opt}}} = 0$ for determining the optimal coefficients can be written as

$$\frac{\partial S}{\partial \vec{\alpha}} \Big|_{\vec{\alpha}=\vec{\alpha}_{\text{opt}}} = -2\vec{b} + 2G\vec{\alpha}_{\text{opt}} = 0. \quad (\text{S4})$$

Thus, $\vec{\alpha}_{\text{opt}}$ is obtained by solving the linear system $G\vec{\alpha}_{\text{opt}} = \vec{b}$ [Eq. (8) in the main text].

B. Scaling of the optimization cost

Assuming a total evolution time T and implementing the time evolution via Trotterization with time step Δt (see the TDVP simulation in section S3), the optimization described in section S1—with the time-dependent Hamiltonian $H[s(t)]$ —is performed at each of the $T/\Delta t$ steps. In the following, we analyze the scaling of the computational cost with system size N for a single step for both the global optimization and local optimization schemes (see the main text for descriptions of these two schemes), focusing on geometrically local Hamiltonian path on finite-dimensional lattices.

1. Global optimization

For each step, the global optimization consists of two parts: (i) computing the elements of G and \vec{b} , and (ii) solving the linear system $G\vec{\alpha}_{\text{opt}} = \vec{b}$.

For a geometrically local Hamiltonian path, nested commutators of the local terms [Eq. (6) in the main text] that do not spatially overlap vanish. Consequently, the total number of variational coefficients associated with the non-vanishing terms scales as $\dim(\vec{\alpha}) = O(N)$. Therefore, the matrix G contains $O(N^2)$ elements, while the vector \vec{b} contains $O(N)$ elements.

Using the geometric locality of the Hamiltonian once again, one can show that the commutators $\{C_\eta\}$ are also geometrically local, and each can be evaluated in $O(1)$ time. Combining the locality of $\{C_\eta\}$ with Eq. (S3), it follows that each element of G and \vec{b} can likewise be evaluated in $O(1)$ time.

In summary, the computational cost of part (i) is dominated by evaluating the elements of G , which scales as $O(N^2)$. For part (ii), solving a linear system of dimension $O(N)$ generally requires $O(N^3)$ computational cost. Therefore, the overall asymptotic computational cost of the global optimization per step scales as $O(N^3)$.

2. Local optimization

In the local optimization scheme, we partition the system into $O(N)$ geometrically local regions $\{\mathcal{B}_\mu\}$ that cover the full lattice. For each region \mathcal{B}_μ , we define $H_{\mathcal{B}_\mu}$ as the sum of all Hamiltonian terms in H that are supported within \mathcal{B}_μ . Similarly, we construct $\mathcal{A}_{\text{WNC}}^{(\ell, \mathcal{B}_\mu)}$ by summing the nested commutators of local terms supported in \mathcal{B}_μ . We then construct the action in the same manner as in Eq. (S1), but with the Hamiltonian and the WNC ansatz replaced by their local counterparts, $H_{\mathcal{B}_\mu}$ and $\mathcal{A}_{\text{WNC}}^{(\ell, \mathcal{B}_\mu)}$.

Following the same procedure as in section S1, together with the scaling analysis for the global optimization case in section S1 B 1, one finds that $O(N)$ individual optimizations are required, one for each local region. However, the computational cost of each local optimization scales as $O(1)$. Therefore, the total computational cost per evolution step for the local optimization approach scales as $O(N)$.

Compared to the global optimization scheme, whose single-step computational cost scales as $O(N^3)$, the local optimization approach significantly reduces this overhead to $O(N)$. Moreover, although the local optimization is expected to yield suboptimal solutions with respect to minimizing the global action in Eq. (S1), this does not necessarily imply a lower state-preparation fidelity compared to the global optimization scheme. In fact, as shown in the main results, the local optimization achieves an infidelity comparable to that obtained via global optimization.

S2. 2D AKLT STATE ON THE HEXAGONAL LATTICE

The 2D AKLT state of spin- $S = 3/2$ on the hexagonal lattice can be expressed as a PEPS with bond dimension $D = 2$, as illustrated in Fig. 1(a) in the main text. Each bulk operator Q_v consists of a projector $P_{S,v}$ and a singlet matrix $Y = \begin{pmatrix} 0 & -1 \\ 1 & 0 \end{pmatrix}$, where $P_{S,v}$ projects the n_v qubits at vertex v onto their symmetric subspace, and each Y transforms a virtual entangled pair into a singlet [S2]. For the hexagonal lattice, the bulk operator takes the form $Q_v = P_{3/2,v} (\mathbb{1} \otimes Y \otimes Y)$. The local projector $P_{3/2,v}$ is explicitly given by

$$\begin{aligned} P_{3/2,v} &= |000\rangle\langle 000| + |111\rangle\langle 111| \\ &+ \frac{1}{3} (|011\rangle + |101\rangle + |110\rangle)(\langle 011| + \langle 101| + \langle 110|) \\ &+ \frac{1}{3} (|001\rangle + |010\rangle + |100\rangle)(\langle 001| + \langle 010| + \langle 100|). \end{aligned} \quad (\text{S5})$$

Here, the virtual qubits in the AKLT construction are promoted to physical qubits. In the 2D hexagonal lattice case, each site hosts $n_v = 3$ qubits, and the physical spin-3/2 degree of freedom corresponds to the symmetric subspace with basis states

$$|S_z = +\frac{3}{2}\rangle = |000\rangle, \quad (\text{S6})$$

$$|S_z = +\frac{1}{2}\rangle = \frac{1}{\sqrt{3}}(|001\rangle + |010\rangle + |100\rangle), \quad (\text{S7})$$

$$|S_z = -\frac{3}{2}\rangle = |111\rangle, \quad (\text{S8})$$

$$|S_z = -\frac{1}{2}\rangle = \frac{1}{\sqrt{3}}(|011\rangle + |101\rangle + |110\rangle). \quad (\text{S9})$$

S3. NUMERICAL SIMULATION DETAILS

We use matrix product states (MPS) to represent the quantum state during both the adiabatic and counterdiabatic dynamics. For the 2D hexagonal lattice with cylindrical boundary conditions [cf. Fig. 1(c) in the main text], we adopt a 1D snake ordering to label the lattice sites (see the Supplementary Material of Ref. [S3]).

The time-dependent variational principle (TDVP) [S4, S5] is employed to evolve the MPS during the adiabatic and counterdiabatic dynamics. To compute $\partial_s h_j$ needed for constructing the local terms within the WNC ansatz [cf. Eq.(6) in the main text], we use a finite-difference approximation,

$$\partial_s h_j(s) \approx \frac{h_j(s + \Delta s) - h_j(s - \Delta s)}{2\Delta s}, \quad (\text{S10})$$

where $\Delta s = 0.01$ is sufficient to ensure numerical convergence.

All simulations are carried out using the TDVP implementation in the `ITensor.jl` library [S6]. We set the single-step simulation error per MPS bond to $\delta = 10^{-9}$ (1D MPS), $\delta = 2 \times 10^{-8}$ (2D AKLT), and the time step to $dt = 0.05$ (δ and dt are the parameters of the TDVP function within `ITensor.jl`), which are sufficient to obtain converged results.

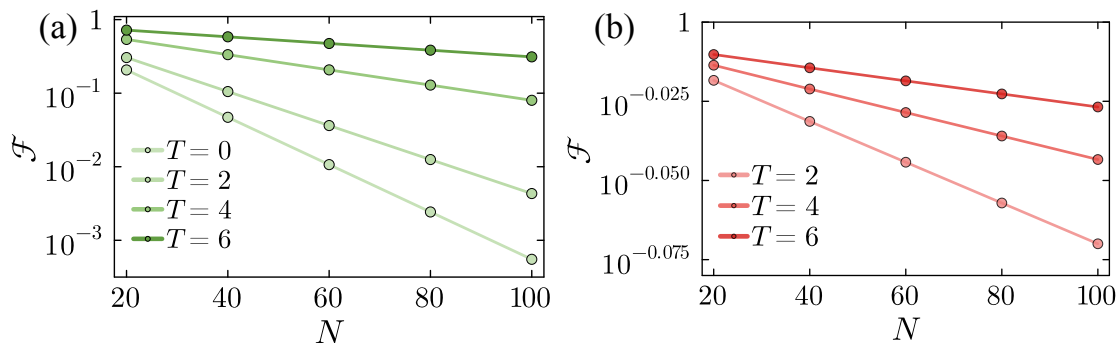


FIG. S1. The fidelity \mathcal{F} for preparing a 1D MPS with correlation length $\xi \approx 2.5$, shown as a function of system size N for various evolution times T , using (a) adiabatic evolution and (b) CD driving with the first-order WNC ansatz.

S4. ADDITIONAL RESULTS ON THE PREPARATION OF THE 1D MPS FAMILY

A. Scaling of the Fidelity with system size N

It was shown in Ref. [S3] that, for quasi-adiabatic preparation of the MPS family with evolution time T and system size N , the resulting fidelity exhibits the following scaling behavior [same as Eq. (14) in the main text]:

$$\mathcal{F}(N, T) = \exp[-\kappa(T)N - c(T)], \quad (\text{S11})$$

where $\kappa(T)$ denotes the error density and $c(T)$ is a boundary term that does not scale with the system size N .

This scaling reflects the nature of quasi-adiabatic evolution: residual excitations generated by the finite evolution time act as a finite density of “errors,” leading to an exponential decay of the fidelity with N . Since counterdiabatic (CD) driving suppresses the density of residual excitations throughout the system, we expect the same scaling form to hold for the counterdiabatic evolution at finite time T .

In Fig. S1, we show the scaling of the fidelity \mathcal{F} with system size N for preparing a 1D MPS with correlation length $\xi \approx 2.5$, at various fixed evolution times T , using (a) adiabatic evolution and (b) counterdiabatic (CD) driving with the first-order WNC ansatz. For each fixed T , we find that the fidelity $\mathcal{F}(N, T)$ decays exponentially with N . As T increases, the slope of the exponential decay decreases, indicating that longer evolution times reduce the error density.

This behavior confirms that the scaling form in Eq. (S11) also applies to the counterdiabatic dynamics. From these data, we extract the error density $\kappa(T)$ and the boundary term $c(T)$, as shown in Fig. 3(a,b) of the main text. Furthermore, Fig. 3(c,d) in the main text demonstrates that the scaling form Eq. (S11), with $\kappa(T)$ and $c(T)$ obtained from the finite-size scaling data (cf. Fig. S1) up to $N = 100$, accurately predicts the required evolution time T_p to reach a fixed target fidelity. The prediction agrees with TDVP simulation results up to $N = 1000$, supporting the validity of the scaling form $\mathcal{F}(N, T)$ for large many-body systems.

B. More Results for different correlation lengths, and the boundary term $c(T)$

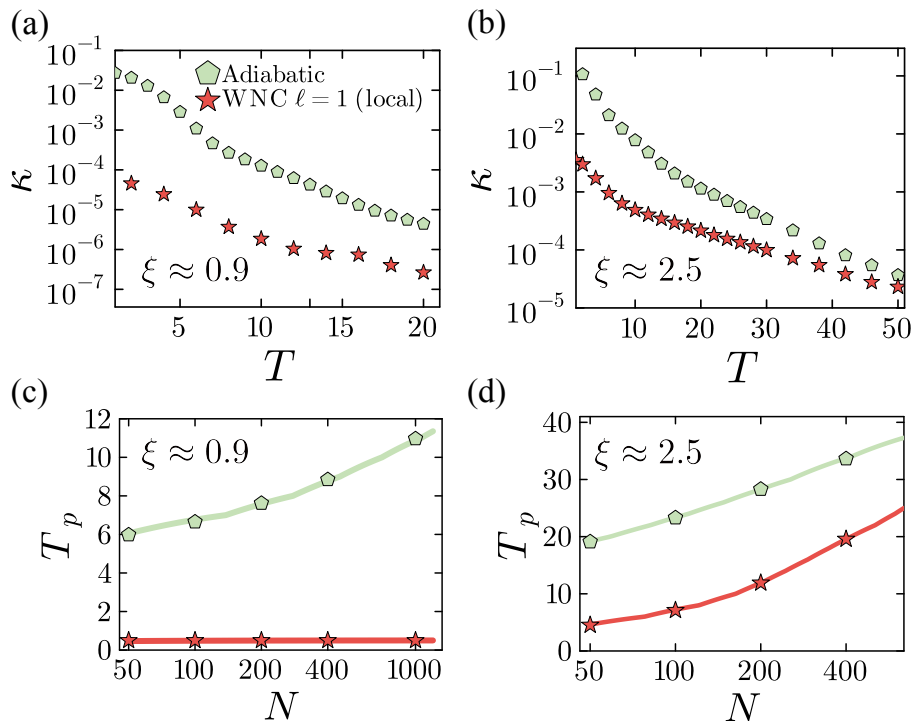


FIG. S2. Preparation of the MPS family with correlation lengths $\xi \approx 0.9$ and 2.5 . (a,b) Extracted error density $\kappa(T)$ [cf. Eq. (S11)] as a function of the evolution time T . (c,d) Required runtime T_p to reach the target fidelity $\mathcal{F} = 0.95$ as a function of system size N . Solid green and red lines indicate the predictions from Eq. (S11), while the symbols denote TDVP simulation results.

In Fig. S2, we present the scaling of the error density $\kappa(T)$ and the required evolution time T_p to reach a target fidelity $\mathcal{F} = 0.95$ for preparing the MPS family with correlation lengths $\xi \approx 0.9$ and $\xi \approx 2.5$. These results complement Fig. 3 in the main text, which shows the cases $\xi \approx 1.6$ and $\xi \approx 3.8$.

In panels (a,b), we observe that CD driving based on the first-order WNC ansatz significantly reduces the error density $\kappa(T)$. For the small correlation length case $\xi \approx 0.9$, $\kappa(T)$ at short evolution times is reduced by nearly three orders of magnitude. This substantial suppression of the error density translates into a markedly reduced preparation time T_p for system sizes up to $N = 1000$.

Panels (c,d) further demonstrate that the WNC approach significantly lowers the required evolution time T_p . Notably, for $\xi \approx 0.9$, the WNC protocol yields such a small error density that the required time T_p shows almost no scaling with N up to $N = 1000$ in order to reach the target fidelity $\mathcal{F} = 0.95$. Moreover, the TDVP simulation results are in good agreement with the T_p predicted from the scaling form Eq. (S11).

Finally, in Fig. S3, we plot the boundary term $c(T)$ for both adiabatic evolution and the first-order WNC protocol at different correlation lengths $\xi \approx 0.9, 1.6, 2.5$, and 3.8 . We observe that $c(T)$ remains small over the entire range of evolution times T . Moreover, the WNC approach consistently reduces this boundary error term compared to adiabatic evolution at each fixed T .

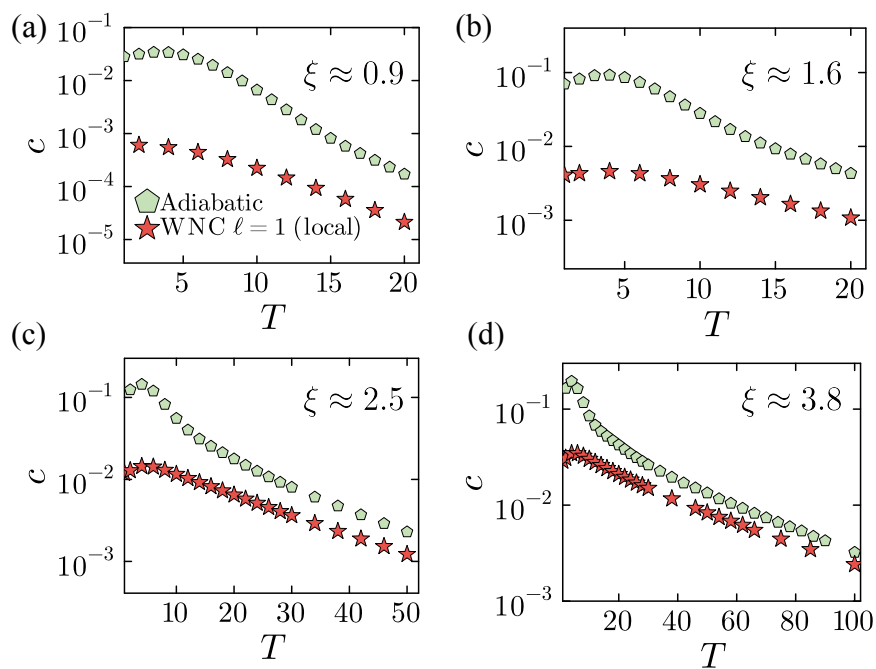


FIG. S3. Extracted boundary term $c(T)$ [cf. Eq. (S11)] versus the evolution time T for the preparation of the MPS family with correlation lengths $\xi \approx 0.9, 1.6, 2.5, 3.8$.

C. Comparing gate costs in Trotterized simulations of various state-preparation schemes

As shown in Fig. 2 of the main text, the first-order WNC ansatz already achieves a lower state-preparation infidelity than high-order NC ansatz. Moreover, implementing the first-order WNC ansatz experimentally is expected to be substantially easier than realizing high-order NC ansatz. To make this point explicit, we evaluate the gate cost of the digital Hamiltonian simulation of the Hamiltonian paths $H[s(t)]$ (adiabatic) and $H_{\text{CD}}[s(t)]$ (CD, for various ansätze, including first-order WNC and high-order NC) [cf. Eqs. (1) and (2) in the main text].

For the time-dependent Hamiltonian, we discretize the evolution into N_{steps} intervals of duration τ , such that the total evolution time is $T = N_{\text{steps}}\tau$. The first-order product-formula approximation is defined as

$$U_{\text{Trotter}}(T) = \prod_{k=1}^{N_{\text{steps}}} \prod_{j=1}^{N_h} e^{-i\tau h_j[s(k\tau)]}, \quad (\text{S12})$$

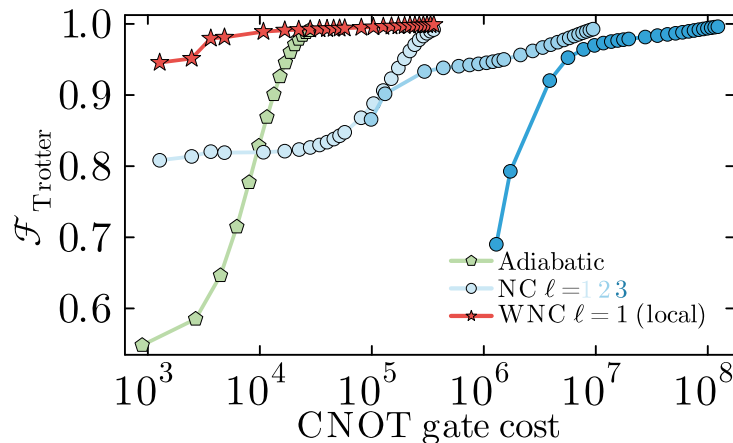


FIG. S4. Preparation of the 1D MPS family with correlation length $\xi \approx 3.8$, system size $N = 6$, using the adiabatic protocol and CD driving with various ansatz. Fidelity as a function of the total CNOT gate count using the first-order trotterized evolution [cf. Eq. (S12)].

where $h_j[s(k\tau)]$ denotes the j -th local term of the Hamiltonian at time $k\tau$. Applying this Trotterized evolution to the initial state $|\psi(0)\rangle$, we obtain the Trotterized final state $|\phi'(T)\rangle$ [cf. near Eq. (13) in the main text]. We then use the fidelity $\mathcal{F}_{\text{Trotter}} = |\langle\psi(1)|\phi'(T)\rangle|^2$ to quantify the performance of the digital state preparation. Note that Trotter errors are expected to reduce $\mathcal{F}_{\text{Trotter}}$ and are therefore already taken into account in our analysis.

We focus on estimating the gate cost of preparing the MPS family. Because the local terms of the MPS parent Hamiltonian [Eq.(13) in the main text] typically do not admit a simple Pauli-string decomposition, we treat each $e^{-i\tau h_j[s(k\tau)]}$ as a generic m -qubit unitary, where m denotes the support size of the local term $h_j(s)$. Implementing such a generic m -qubit unitary requires at most $N_{\text{CNOT}}^{(m)} = \lceil \frac{1}{4}(4^m - 3m - 1) \rceil$ CNOT gates [S7], which we use as our estimate of the CNOT cost for each unitary. The total CNOT gate cost is then obtained by summing the costs of all unitaries within $U_{\text{Trotter}}(T)$ [cf. Eq. (S12)].

In Fig. S4, we show the fidelity $\mathcal{F}_{\text{Trotter}}$ as a function of the CNOT gate cost for preparing the MPS family with correlation length $\xi \approx 3.8$ and system size $N = 6$, using the schedule function $s(t) = \sin^2 \left[\frac{\pi}{2} \sin^2 \left(\frac{\pi t}{2T} \right) \right]$. We fix the time step to $\tau = 0.05$ and vary N_{step} to change the total evolution time T ; accordingly, the CNOT gate cost also varies. The choice of a constant time step is motivated by current near-term quantum devices, where the Trotter step size is typically taken to be constant.

From Fig. S4, we see that at a relatively low CNOT gate cost of $\sim 10^3$, counterdiabatic driving based on the first-order WNC ansatz already achieves a high fidelity of $\mathcal{F}_{\text{Trotter}} \approx 0.94$. By contrast, the adiabatic protocol requires roughly an order of magnitude more CNOT gates to reach a comparable fidelity. Moreover, the high-order NC ansatz require substantially more CNOT gates to achieve similar performance, and in fact perform even worse than the adiabatic protocol because of the large overhead associated with high-order nested commutators. These results therefore highlight that the first-order WNC ansatz not only substantially accelerates the adiabatic evolution, but also introduces only a modest overhead comparable to that of the first-order NC ansatz. As a result, it provides the most resource-efficient approach for preparing the target state to a given high fidelity.

-
- [S1] D. Sels and A. Polkovnikov, Minimizing irreversible losses in quantum systems by local counterdiabatic driving, *Proceedings of the National Academy of Sciences* **114**, E3909 (2017).
- [S2] J. I. Cirac, D. Pérez-García, N. Schuch, and F. Verstraete, Matrix product states and projected entangled pair states: Concepts, symmetries, theorems, *Rev. Mod. Phys.* **93**, 045003 (2021).
- [S3] Z.-Y. Wei, D. Malz, and J. I. Cirac, Efficient adiabatic preparation of tensor network states, *Phys. Rev. Res.* **5**, L022037 (2023).
- [S4] J. Haegeman, J. I. Cirac, T. J. Osborne, I. Pizorn, H. Verschelde, and F. Verstraete, Time-dependent variational principle for quantum lattices, *Phys. Rev. Lett.* **107**, 070601 (2011).
- [S5] J. Haegeman, C. Lubich, I. Oseledets, B. Vandereycken, and F. Verstraete, Unifying time evolution and optimization with matrix product states, *Phys. Rev. B* **94**, 165116 (2016).

- [S6] M. Fishman, S. R. White, and E. M. Stoudenmire, The ITensor Software Library for Tensor Network Calculations, [SciPost Phys. Codebases](#) , 4 (2022).
- [S7] R. Iten, R. Colbeck, I. Kukuljan, J. Home, and M. Christandl, Quantum circuits for isometries, [Phys. Rev. A](#) **93**, 032318 (2016).